Thirumurugan, S. et al. (2022) Angiopep-2-decorated titanium-alloy core-shell magnetic nanoparticles for nanotheranostics and medical imaging. *Nanoscale*, 14(39), pp. 14789-14800. (doi: 10.1039/d2nr03683e)

There may be differences between this version and the published version. You are advised to consult the published version if you wish to cite from it. https://doi.org/10.1039/D2NR03683E

https://eprints.gla.ac.uk/282444/

Deposited on 22 November 2022

Enlighten – Research publications by members of the University of Glasgow
http://eprints.gla.ac.uk

Angiopep-2-decorated Titanium-Alloy Core-Shell Magnetic Nanoparticles for Nanotheranostics and Medical Imaging

Senthilkumar Thirumurugan [1,†], Pranjyan Dash [1,†], Xinrui Liu [2,†], Yuan-Yun Tseng [3], Wei-Jhih Huang [1], Yunqian Li [2], Gang Zhao [2], Chingpo Lin [2], Murugan Keerthi [1], Udesh Dhawan [4*], Ren-Jei Chung [1*]

[1] Department of Chemical Engineering and Biotechnology, National Taipei University of Technology (Taipei Tech), Taipei 10608, Taiwan

[2] Department of Neurosurgical Oncology, First Hospital of Jilin University, Changchun, China

[3] Department of Neurosurgery, New Taipei Municipal TuCheng Hospital (Built and Operated by Chang Gung Medical Foundation), New Taipei City 236017, Taiwan

[4] Centre for the Cellular Microenvironment, University of Glasgow, Scotland, UK

† These authors contribute equally to this paper.

* Corresponding Author: Dr. Ren-Jei Chung

Email: rjchung@mail.ntut.edu.tw; Tel: (886-2) 2771-2171 ext. 2547

Address: Department of Chemical Engineering and Biotechnology, National Taipei University of Technology (Taipei Tech), No. 1, Sec. 3, Zhongxiao E. Rd., Taipei 10608 Taiwan.

Also correspondence to Dr. Udesh Dhawan (Udesh.dhawan@glasgow.ac.uk).

Table of contents (TOC)

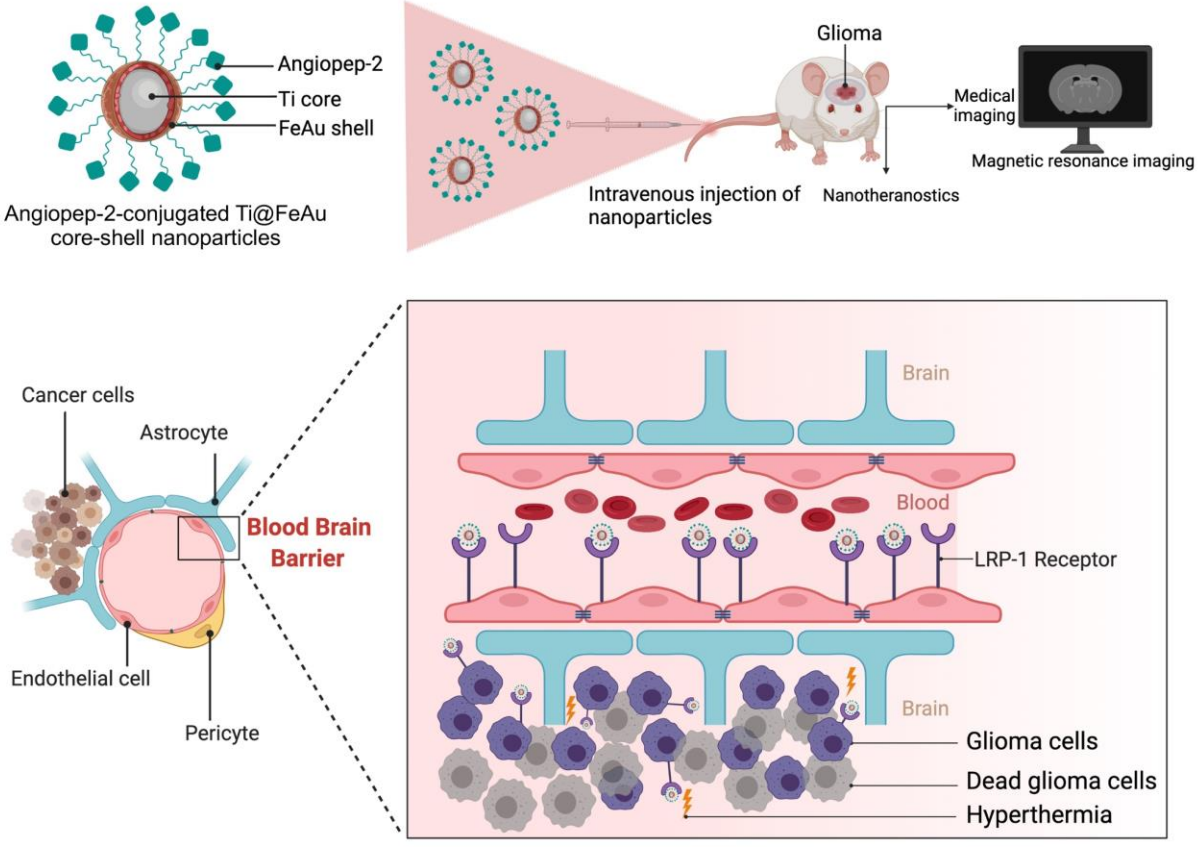

ABSTRACT

The poor permeability of therapeutic agents across the Blood-Brain barrier and Blood-Tumor Barrier is a significant barrier in glioma treatment. Low-density lipoprotein receptor-related protein (LRP-1) recognises a dual-targeting ligand, Angiopep-2, which is over-expressed on BBB and Gliomas. Here, we have synthesized Ti@FeAu core-shell nanoparticles conjugated with Angiopep-2 (Ti@FeAu-Ang Nanoparticles) to target glioma cells and treat brain cancer via hyperthermia produced by a magnetic field. Our results confirmed that Ti@FeAu core-shell Nanoparticles were superparamagnetic, improved negative contrast effect on glioma, and exhibited a temperature elevation of 12 ° C upon magnetic stimulation, which implies potential applications in magnetic resonance imaging (MRI) and hyperthermia-based cancer therapy. Angiopep-2-decorated nanoparticles exhibited higher cellular uptake by C6 glioma cells than by L929 fibroblasts, demonstrating selective glioma targeting and improved cytotoxicity up to 85% owing to hyperthermia produced by magnetic field. The *in-vivo* findings demonstrated that intravenous injection of Ti@FeAu-Ang Nanoparticles exhibited a 10-fold decrement in tumor volume compared to the control group. Furthermore, immunohistochemical analysis of Ti@FeAu-Ang Nanoparticles showed coagulative necrosis of tumor tissues and preliminary safety analysis highlighted no toxicity to the haematological system, after Ti@FeAu-Ang Nanoparticles-induced hyperthermia treatment.

KEYWORDS: gliomas, angiopep-2, theranostics, hyperthermia, titanium, iron-gold nanoparticles.

1. Introduction

Gliomas are the most prominent central nervous system tumor in humans, originating from glial cells of the brain, and causes second-highest number of deaths[1]. Chemotherapy is a clinically accepted way of treating gliomas due to the ineffectiveness of traditional surgical resection in preventing glioma penetration into adjacent normal tissue. The treatment of gliomas is very complicated due to its complex microenvironment[2] and is a key challenge to effectively deliver the therapeutic agents to tumor and to sensitive cells not located in the tumor bed[3]. The therapeutic effects of drugs are restricted in the brain tumor region and, also frequently produce side effects. Almost all therapeutic agents, large or small, struggle to reach brain tumors owing to two main reasons[4]. First, Blood-Brain Barrier (BBB) is the major obstacle for the delivery of nanoparticles or drugs to the tumor site in the brain[5]. This is because of the tight linking of endothelial cells and diverse kind of efflux transporters at the BBB[6]. Within the tumor, the BBB is compromised and is limited to the tumor bed[7]. The second significant barrier is the blood−tumor barrier (BTB), which also controls the penetrability of nanoparticles from blood to tumor due to the high internal pressure of the tumor[8]. Compared to the BTB of peripheral tumors, the BTB of visceral tumors is tighter due to the transporter expression, transendothelial fenestrations, and inter-endothelial cell gaps[9]. Nanoparticles are considered an effective carrier for delivering drugs to the tumor region due to the enhanced permeability and retention (EPR). However, in case of a brain tumors, it is difficult for the nanoparticles and drugs to reach the brain tumor region due to a lack of vessels[10]. Hence, the cell-penetrating peptides (CPPs) can be conjugated to nanoparticles due to their ability to cross the BBB[11]. However, the selectivity of CPPs is hampered between neoplastic and non-neoplastic cells[12, 13]. Interestingly, it was found that low-density lipoprotein receptor-related protein-1 (LRP-1) expression was higher in glial cells than in normal cells[4]. Accordingly, Angiopep-2 can be selected for dual-targeting delivery to the BBB and glioma cells, and its receptor-mediated mechanism has been extensively studied elsewhere[14]. Angiopep-2, a 19-amino

acid peptide ligand, is derived from the Kunitz domain of aprotinin[15], displays strong affinity for LRP-1 and has been previously employed for glioma-targeting[16]. Therefore, in this study, we employed angiopep-2 for BBB penetration and glioma targeting.

Magnetic hyperthermia therapy (MHT) is a highly promising therapeutic strategy for treating various cancers because of its remarkable effectiveness, low cost, non-invasiveness, minimized damage to normal tissues, and excellent tissue penetrability[17, 18]. MHT is approved in Europe to treat brain tumors; however, there are limited clinical trials. Typically, magnetic nanoparticles (MNPs) are delivered to cancer cells to generate a considerable amount of heat upon exposure to an alternating magnetic field (AMF) [19]. This is due to the energy loss processes such as Néel and Brownian relaxation and hysteresis loss of the nanoparticles[20, 21]. Besides, in this treatment, heat is generated only in the areas containing nanoparticles, and AMF can penetrate tumors that are deeply located within the body[22, 23]. In general, cancer cells are more sensitive to hyperthermia than normal cells[24] and undergo apoptosis when exposed to elevated temperatures between 42-46 °C. In contrast, healthy cells can survive this temperature range[25]. It has also been validated that magnetic hyperthermia at suitable temperatures increases the susceptibility of cancer cells to chemotherapy, radiation, and immunotherapy[25]. The poor permeability of therapeutic agents across the Blood-Brain barrier and Blood-Tumor Barrier greatly is a significant barrier in glioma treatment. There are several techniques for inducing hyperthermia, including radiofrequency, infrared radiations, and tubes with a hot water bath. However, these techniques are unsuitable due to their side effects. Thus, magnetic hyperthermia is an advantageous therapy to disperse nanoparticles throughout the affected tissue via the application of an external alternating current magnetic field. Magnetic hyperthermia has gained widespread recognition for the following reasons:

1. Capacity for targeted, homogeneous, and controlled heat generation.

2.Capacity to reach deep-rooted tumors.

3. Capability to specifically target the tumor vasculature.

Nanoparticles have also been extensively utilized in various biomedical applications[19] owing to their optical properties, low cost, simple synthesis process, low toxicity, biocompatibility, and unique magnetic properties[26]. Moreover, theranostic purposes of the nanoparticles are also explored as MRI contrast agents, imaging agents, targeted drug delivery, hyperthermia, and bio-sensing[27-29]. Iron-gold (Fe-Au) alloy Nanoparticles have gained significant scientific attention in various biological applications such as medical imaging, magnetic separation, and nanotheranostics because of their exceptional magnetic properties[30]. Recently, Ti and its corresponding alloys have emerged as attractive biomaterials[31]. These are widely employed in biomedical applications owing to their remarkable biocompatibility[32, 33]. Additionally, Ti nanoparticles also display some unique physical properties such as high corrosion resistance, stable thermodynamic state in the physiological environment, and less ion formation in water and other aqueous media[34]. Despite its attractive properties, to the best of our knowledge there are only a handful of studies exploring the suitability of Titanium in cancer therapeutics. Out of the existing studies, the application of titanium has only been explored for photothermal treatment to limit tumour growth. As shown by Behnam et al., photothermal treatment generated by Titanium displayed limited tumor decrement, providing scope for improvement of Titanium-based models for cancer theranostics[35]. Thus, the suitability of Titanium to limit cancer growth via magnetic hyperthermia remains unvalidated. To this end, this study validates the effectiveness of Titanium-generated magnetic hyperthemia in cancer theranostics by limiting glioma growth.

In this work, Ti@FeAu core-shell Nanoparticles were conjugated with Angiopep-2 for specific ingestion by gliomas. These magnetic nanoparticles can also be used to generate heat upon AMF stimulation to induce cancer cell death. In this regard, Ti@FeAu core-shell nanoparticles were successfully prepared via micro-emulsion method and conjugated to Angiopep-2 to synthesize Ti@FeAu-Ang nanoparticles. We provide a detailed explanation of (a) capability of

this Ti@FeAu-Ang Nanoparticles complex to limit glioma cell growth *in-vitro* via hyperthermia, (b) efficiency of Ti@FeAu-Ang nanoparticles limiting glioma development in a rat model upon AMF treatment (c) Application of Ti@FeAu-Ang Nanoparticles for medical imaging. Furthermore, Ti@FeAu-Ang nanoparticles specifically target glioma, trigger cancer cell apoptosis and improve tumor imaging by improving image contast, thereby making it is a promising platform for theranostics.

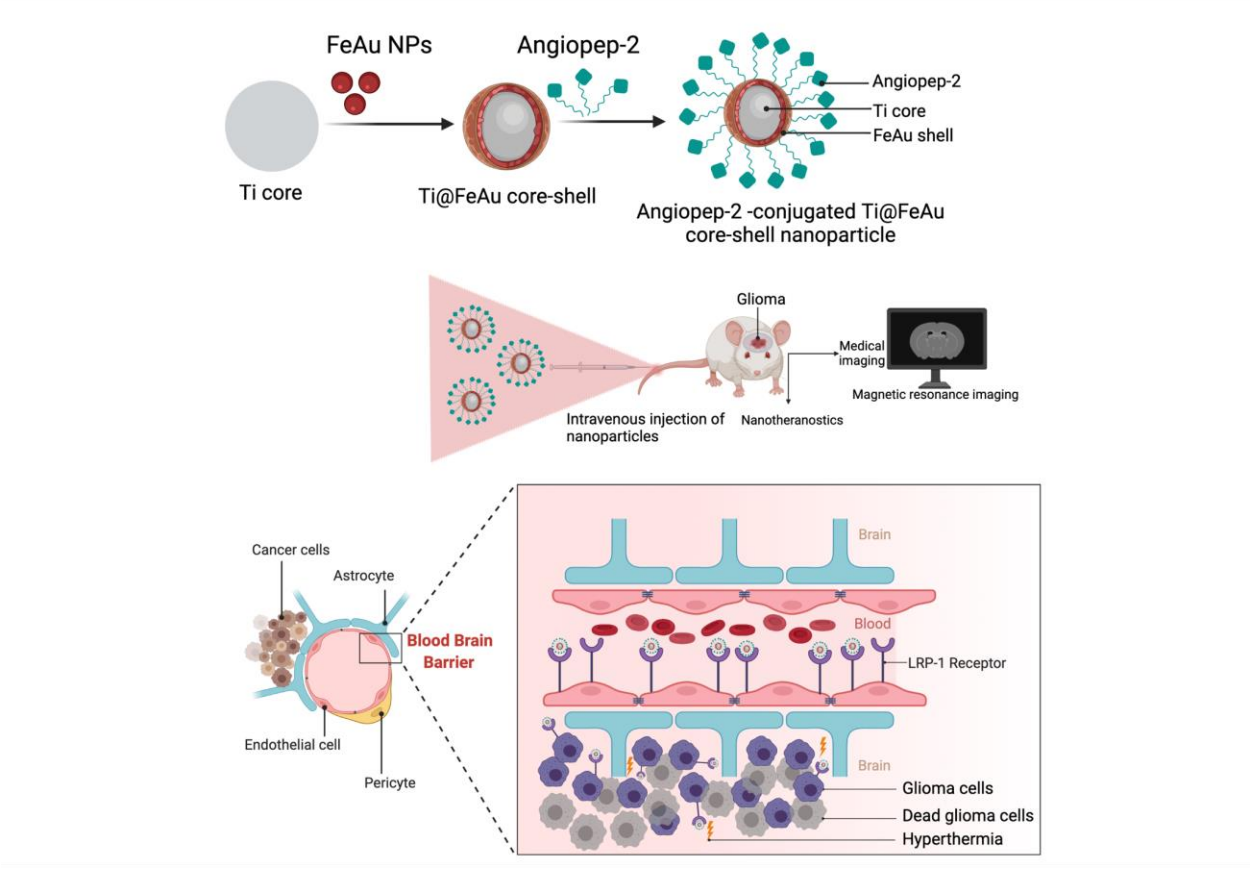

Scheme 1. Schematic representation of synthesis of Angiopep-2-decorated Ti@FeAu core-shell nanoparticles. The conjugation with Angiopep-2 enables crossing BBB and target glioma cells upon AMF stimulation.

2. Experimental

2.1. Material and Characterization

Titanium powder, Sodium borohydride, Tetrachloroauric (III) acid trihydrate, Cetyl Trimethyl Ammonium Bromide (CTAB), 1-Butanol, N-Octane, absolute ethanol, and all other chemicals were purchased from Sigma (USA). Angiopep-2 (TFFYG-GSRGKRNNFKTEEYC) ＞ 99.8% was purchased from Qunda Marine Technology Co., Ltd. The morphology of nanoparticles was assessed using Transmission electron microscopy (TEM) and the particle size and surface potential were analyzed using Image J and Zetasizer, respectively. X-Ray Diffraction (XRD) spectroscopy was used to study crystal structure of the Ti@FeAu Nanoparticles and Energy Dispersive X-Ray Spectroscopy (EDS) was utilized to study the composition. UV spectrophotometer (SP-8001/Yoyu) was used to confirm decoration of Angiopep-2 with Ti@FeAu Nanoparticles and the magnetic properties were analyzed using superconducting quantum interference device (SQUID).

2.2. Synthesis of Ti@FeAu core-shell Nanoparticles

Ti@FeAu core-shell nanoparticles were prepared via microemulsion method. Argon gas was first purged into a three-necked flask. Then, 0.2 M of $FeSO_4$ and 0.5 M of $NaBH_4$ solution were taken in two separate centrifuge tubes, and micro-emulsion of $FeSO_4$ and $NaBH_4$ was prepared by adding 1.699 g of CTAB, 2.485 mL of 1-Butanol, and 0.432 mL of N-Octane in the solution of $FeSO_4$ and $NaBH_4$. Subsequently, three separate centrifuge tubes were taken which contained 0.2 M of pure titanium, 0.2 M of $HAuCl_4$, and 0.8 M of $NaBH_4$ aqueous solution. Similarly, three different microemulsions of titanium, $HAuCl_4$, and $NaBH_4$ were prepared by adding 1.699 g of CTAB, 2.485 mL of 1-Butanol, and 0.432 ml of N-Octane into the above three centrifuge tubes separately. Micro-emulsion containing pure titanium was injected into the three-necked flask using a syringe and stirred for 5 minutes. Micro-emulsion containing 0.2 M of $FeSO_4$ and 0.5 M of $NaBH_4$ was then injected into the three-necked flask using a needle followed by continuous stirring for another 5 minutes. Micro-emulsion containing 0.2 M of $HAuCl_4$ and 0.8 M of $NaBH_4$ was then injected into the three-necked flask using a syringe and stirred for 30 minutes.

The above solution was poured into 50 ml of the centrifuge tube and washed with an appropriate amount of anhydrous alcohol (99.99 %) by centrifugation for 15 minutes at 9000 rpm. The supernatant was removed, and magnetic nanoparticles (MNanoparticles) were collected using a magnet to prevent the collection of Nanoparticles that have not reacted with iron. Again, anhydrous alcohol was added to the centrifuge tube and placed into an ultrasonicator. After centrifuging, the Nanoparticles attached to the tube wall were dispersed into the ethanol and again centrifuged at 9000 rpm for 15 minutes. The above-mentioned steps were repeated three times to wash unreacted microemulsion. Finally, the collected Nanoparticles were dried using a vacuum pump for 4 hours to obtain the black-colored Ti@FeAu Nanoparticles.

2.3. Synthesis of Angiopep-2-decorated Ti@FeAu Nanoparticles

To conjugate Angiopep-2 with Ti@FeAu Nanoparticles, purified Ti@FeAu powder and Angiopep-2 were added into the three-necked flask containing 20 mL PBS. The solution was then subjected to continuous stirring for 24 hours under an inert atmosphere. These mixtures were transferred into a 50 mL centrifuge tube and ultrasonicated to form a homogeneous dispersion. The mixture was then centrifuged and this procedure was repeated several times to remove unconjugated Angiopep-2. Then, the Angiopep-2 conjugated Ti@FeAu Nanoparticles were collected using a magnet. Finally, the powdered Ti@FeAu-Ang Nanoparticles were acquired after the removal of PBS using a vacuum pump.

2.4. Temperature elevation test

Hyperthermia ability of nanoparticles at various concentrations was studied after stimulation using an alternating magnetic field (AMF, 700−1100 kHz) for 10 minutes. Nanoparticleswere prepared at various concentrations ranging from 0.5 to 10 mg mL^{-1} in distilled water. Next, nanoparticles at different concentrations were exposed to AMF, and the temperature was recorded every 30 seconds.

2.5. Analysis of Ti@FeAu-Ang Nanoparticles as a contrast agent

Magnetic resonance spectroscopy was employed to investigate the imaging modality of the Ti@FeAu-Ang Nanoparticles as a contrast agent. For this, various concentration of the Ti@FeAu-Ang Nanoparticles (0, 0.03125, 0.0625, 0.125, 0.25, 0.5 mg mL^{-1}) were prepared by dissolving in 0.5 % of agar and exposed to 7T magnetic resonance spectroscopy (TR-5000ms, TE-60ms). Modification of the T_2 relaxation time was assessed to determine the concentration-dependent fluctuation in contrast.

2.6. Cell culture

L929 mouse fibroblasts and C6 glioma cells were used for this study. L929 and C6 cells were cultured in Dulbecco's Modified Eagle Medium (DMEM) containing 10 % FBS (GIBCO, USA) and antibiotics in a T75 flasks in an incubator maintained at 37 ℃ with a 5% CO_2 atmosphere and 95 % humidity.

2.7. *In-vitro* cytotoxicity

In-vitro cytotoxicity was studied using MTT assay. MTT reagent was diluted 10-fold using complete media and used at 5 mg mL^{-1} concentration. Cells were seeded in multi-well plates for 24 hours after which the culture media was aspirated. Next, 50 µL of MTT reagent in was added to cells and incubated for 4 hours in dark. MTT reagent was then removed and formazan crystals were dissolved by adding 1 mL of DMSO and 200 µL was taken and transferred to 96-well plates. Absorbance was measured at 570 nm. Teflon and latex were used as negative and positive controls, respectively.

2.8 Effect of the magnetic field induced hyperthermia on glioma cells (C6)

C6 cells were seeded at a density of $1x10^5$ cell mL^{-1} for 24 hours after which culture media was removed. Ti@FeAu Nanoparticles and Ti@FeAu-Ang Nanoparticles were sterilized under UV light for 30 minutes, and then 125 µg mL^{-1} concentration of the Nanoparticles were prepared using culture medium. 1 mL of this solution was added to cell culture dish. Then, the above culture dish containing Ti@FeAu Nanoparticles and Ti@FeAu-Ang Nanoparticles was incubated in a CO_2 incubator at 37° C for 4 hours. Next, Nanoparticles were subjected to an alternating magnetic field

stimulation (AMF) for different time points and then placed in the incubator for 24 hours. On the third day, 10-fold diluted MTT reagent was added. After 4 hours, the reagent was discarded, and 1 mL DMSO was added to each well and placed on an orbital shaker at 100 rpm for ten minutes in the dark. Finally, 200 µL of the solution was taken from each dish and the absorbance was measured at 570 nm.

2.9. Assessment of cell-specific Ti@FeAu-Ang Nanoparticles ingestion

To determine the ability of Nanoparticles ingestion in normal (L929 fibroblasts) and cancer cells (C6 glioma), cells were seeded in a 35 mm petri dish at a density of $3x10^5$ cells mL^{-1} and incubated for 24 hours. The next day, purified Ti@FeAu Nanoparticles and Ti@FeAu-Ang Nanoparticles were irradiated with UV light for 30 minutes. Nanoparticles were diluted at a concentration of 125 µg mL^{-1} and added to the petri dish containing cells and incubated for 0.5 or 2 hours. Cells were washed using PBS and then trypsinized and collected via centrifugation. 1 mL of concentrated nitric acid was then added to the cells. DI water was added to dilute the media 10-fold, and elemental composition were determined using inductively coupled plasma-mass spectroscopy (ICP-MS).

2.10. Analysis of nanoparticle ingestion

Intracellular localization of Ti@FeAu-Ang Nanoparticles was studied using optical microscopy. C6 cells were seeded at $3x10^6$ cells mL^{-1} in multi-well culture plate for 24 hours. The following day, Ti@FeAu Nanoparticles and Ti@FeAu-Ang NANOPARTICLES were sterilized under UV light for 30 minutes. The Nanoparticles were then dispersed in DMEM at a concentration of 125 µg mL^{-1} and added to wells containing cells for 24 hours. Cells were then using a mixture of paraformaldehyde (2 %) and Glutaraldehyde (2.5 %) in 0.1 M Cacodylate. The samples were then immersed in PBS followed by dehydration and vacuum drying. The intracellular localization of nanoparticles was analyzed using TEM.

2.11. *In-vivo* assessment using a rat model

Sprague Dawley (SD) rats used for the *in-vivo* experiments were purchased from BioLASCO (Taiwan). Before studies, rats were grown accustomed for a period of seven days. At all times, animals had unlimited access to regular chow and water. All experiments were performed following ; The Institutional Animal Care-approved experimental protocols and Use Committee of Taipei Medical University, under the document number LAC-2017-0485. 30 SD rats weighing 250-300 g were used for the experimental procedure. Zoletil 50 and Rompun (1:2) were prepared, and 0.40 cc was administered for anaesthesia. After providing abdominal anaesthesia to SD rats, the appropriate region of the head was shaved then sterilized with alcohol. Followed by 1.5 cm from the eye, a 2 cm dissection was made with a scalpel, and a hole in the rat's skull was drilled using a high-speed drill bit. Rat stereotactic frame was fixed, and 10 µl of C6 cells (approximately 10^6 cells) were injected into the 1 cm × 1 cm area of soft tissue.

2.12. *In-vivo* imaging test of Ti@FeAu-Ang Nanoparticles

6 to 8 rats with brain tumors were randomly selected, and MRI photographs were taken before injecting the nanoparticles. To investigate the applicability of Ti@FeAu-Ang Nanoparticles as a contrast agent for tumor imaging, Ti@FeAu-Ang Nanoparticles (5 mg mL^{-1}) were prepared in 0.01 M PBS, and 200 µL of Nanoparticles was intravenously injected into the rats bearing brain tumor. A Nb-Fe-B magnet (0.5 T) with a 2 cm x 2 cm diameter was fixed to the rat's skull. After 2 hours of administration, MRI was used to relate the signal intensities of normal and tumor-bearing rats.

2.13. Assessment of tumor growth

To evaluate the effectiveness of Ti@FeAu Nanoparticles and Ti@FeAu-Ang Nanoparticles for cancer theranostics, SD rats were splitted into three groups: control, Ti@FeAu Nanoparticles + AMF (5 mg mL^{-1}), and Ti@FeAu-Ang Nanoparticles +AMF (5 mg mL^{-1}). The control group was administered an intravenous injection of 0.01 M PBS (10 mL kg^{-1}) into the tail. For the other two experimental groups, 200 µL of Ti@FeAu Nanoparticles or Ti@FeAu-Ang Nanoparticles was intravenously injected into the rat tail. A Nb-Fe-B magnet (0.5 T) with a

diameter of 2 cm x 2 cm was fixed to the rat's skull. 2 hours after administration, the rat head was covered with a high-frequency heating coil (700−1100 kHz) for 15 minutes to induce magnetic stimulation. Magnetic therapy was performed weekly, and tumor size was determined on days 0, 7, 14, and 28. The following formula was used to determine the equivalent tumor volume. After 28 days, brain tumor sections were examined to validate the magnetic treatment's effect on the brain tumors.

2.14. Immunohistochemical Analysis

After treatment, brain tissues and main organs such as the heart, liver, spleen, lungs, and kidney were dissected from tumor-bearing rats. The brain tissues were treated in formalin (10 %) before implantation in paraffin. Then, the tissues were cut into 5 mm thick fragments, stained with Haematoxylin & Eosin (H&E), and observed under an optical microscope.

2.15. Statistical analysis

All experiments were performed atleast thrice independently using the nanoparticles. The data is represented as mean with standard deviations. Graphs were plotted using Origin, and Prism 9 was used to perform statistical analysis. Kruskal-Wallis test with Dunn's multiple comparison or one-way ANOVA was utilized to identify datasets that were statistically different. Significant data sets with p-value <0.05 are represented with * and those with p-value <0.01, <0.001and <0.0001 were represented with **, *** or ***, respectively.

3. Results and discussion

3.1. Characterization of Ti@FeAu core-shell Nanoparticles

The morphological characterization of Ti, FeAu, and Ti@FeAu Nanoparticles was performed using TEM. (Figure 1a) displays that the Ti Nanoparticles exhibit a spherical shape with an average diameter of 100 nm. Low and high magnification TEM images of the FeAu alloy Nanoparticles with different magnifications are presented in **(**Figure 1b,c) which indicate the

synthesis of spherical-shaped FeAu Nanoparticles. (Figure 1d,e) show (low and high magnification) TEM images of the Ti@FeAu Nanoparticles. During the synthesis process, the FeAu layer covered the Ti Nanoparticles resulting in Ti@FeAu core-shell Nanoparticles. From the particle size distribution analysis of Ti@FeAu Nanoparticles (Figure 1f), the average particle size of Ti@FeAu Nanoparticles was calculated to be 127.99 ± 23.57 nm. Additionally, EDS analysis was performed to determine the presence of titanium (Ti), iron (Fe), and gold (Au) in the Ti@FeAu Nanoparticles (Figure 1g). As shown in (Figure 1h), the elements such as Ti, Fe, and Au were presented with the weight percentage of 22.66, 5.7, and 71.64 %, respectively.

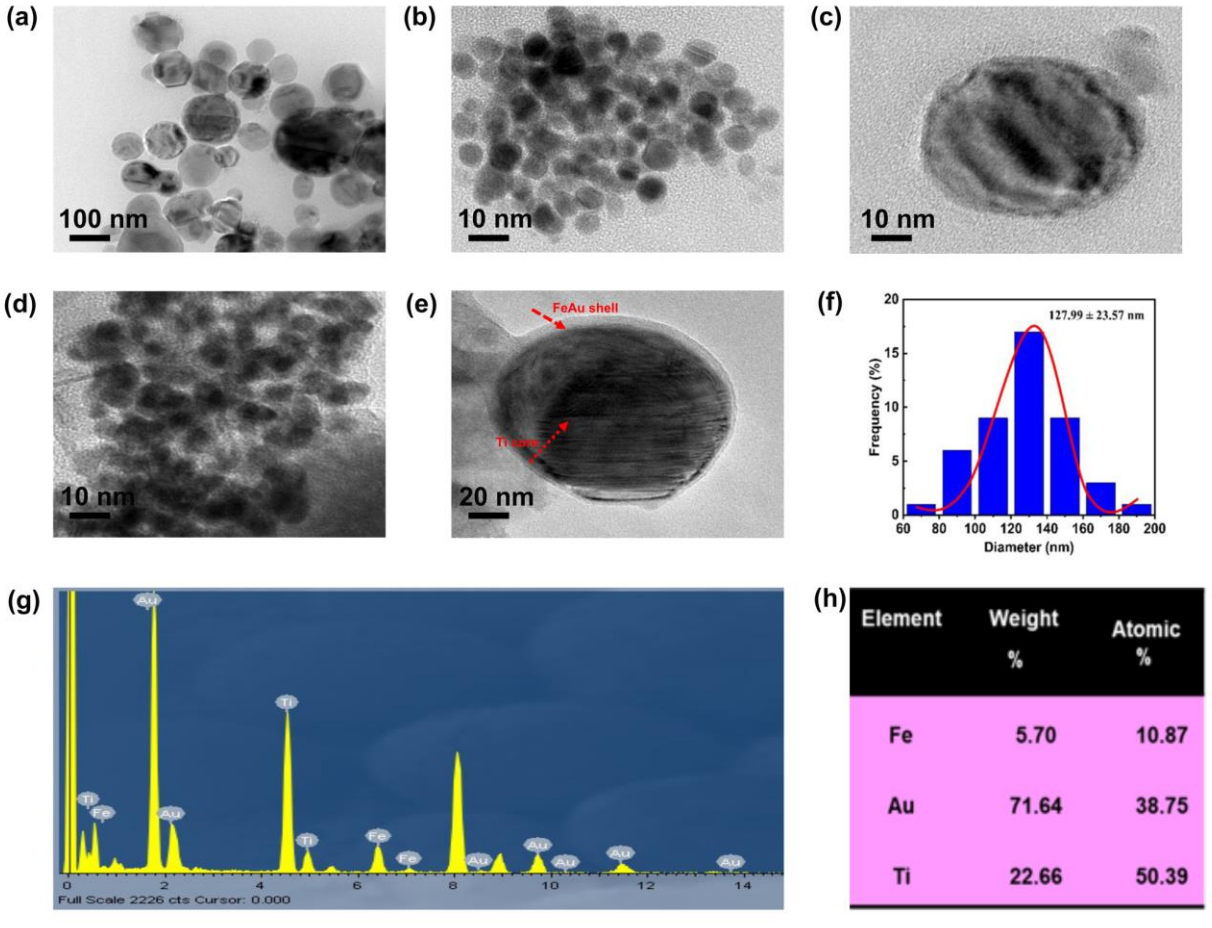

Element	Weight %	Atomic %
Fe	5.70	10.87
Au	71.64	38.75
Ti	22.66	50.39

Figure 1. Characterization of Ti@FeAu core-shell Nanoparticles. (a) TEM micrographs of Titanium Nanoparticles, (b and c) TEM micrographs of FeAu Nanoparticles (low and high magnification), (d and e) TEM micrographs of Ti@FeAu core-shell Nanoparticles (low and high

magnification), (f) particle size distribution of Ti@FeAu core-shell Nanoparticles, (g) EDS analysis of Ti@FeAu Nanoparticles (h) the elemental weight percentage of Fe, Au and Ti.

X-ray diffraction (XRD) spectroscopy was used to analyse the crystalline structure of the nanoparticles (Figure 2a). The XRD pattern highlighted that the prominent peaks obtained at 2θ values of 44.7° and 65.1° correspond to the crystal plane of (110) and (200), indicating the body-centered cubic (BCC) structure of Fe (JCPDS 00-006-0696)[37]. The 2θ peaks at 44.7°, 65.1° and 77.7° corresponded to the crystal plane of (111), (220), and (311) indicate the face-centered cubic (FCC) structure of Au (JCPDS 03-065-2870)[38]. An additional peak with a 2θ value of 40.8° corresponds to the (101) plane of Ti@FeAu Nanoparticles, which is evident of the FeAu layer formation over the Ti core[39]. Moreover, no additional peaks correspond to iron oxide and titanium oxide, which confirms that the Ti@FeAu alloy Nanoparticles were not oxidized.

The conjugation of Angiopep-2 to Ti@FeAu Nanoparticles was confirmed by FTIR analysis (Figure 2b). FTIR analysis of Ti@FeAu-Ang Nanoparticles showed the individual functionalities of Angiopep-2 and Ti@FeAu-Ang Nanoparticles, demonstrating the effective conjugation of Angiopep-2 with Ti@FeAu Nanoparticles. The band observed at 1045 cm^{-1} attributes to stretching vibration of C–O. Additionally, the bands at 1538 cm^{-1} and 1646 cm^{-1} correspond to N-H, and C=O bonds, respectively [40]. As shown in (Figure 2c), the Raman spectra of Ti@FeAu-Ang Nanoparticles display an absorption peak between 290 cm^{-1} and 330 cm^{-1}. According to the literature, the wavelength of 290 cm^{-1} is the characteristic peak for Au-S [41]. The absorption peak of the Au-S bonds is recognized from gold in the Ti@FeAu Nanoparticles, which is bonded to the thiol group of cysteine on Angiopep-2. This result further proves that Angiopep-2 was successfully conjugated to Ti@FeAu Nanoparticles. The surface potential (Zetasizer) was analyzed to assess changes in the surface potential of Ti@FeAu Nanoparticles after conjugation with Angiopep-2 at a concentration of 1 mg mL^{-1} at a fixed pH of 7. The surface potential of Ti@FeAu Nanoparticles was found to be 31.3 ± 0.4 mV at pH 7. After modification with the

Angiopep-2, the surface potential of Ti@FeAu Nanoparticles increased from -31.3 ± 0.4 to -15.03 ± 0.38 mV. We note that the difference in the zeta potential between Ti@FeAu and Ti@FeAu-Ang Nanoparticles was not statistically significant. The rise in potential after angiopep-2 conjugation has been described before, therefore our findings are in line with the earlier research[42]. Likewise, the surface potential of Angiopep-2-decorated Ti@FeAu Nanoparticles was negative, which indicated that Ang-Ti@FeAu Nanoparticles were safe for biological research. This is because the negatively charged Nanoparticles can avoid the activation of immune response by monocytes and macrophages in the bloodstream[43]. The results are shown in (Table 1) and (Figure 2d) From these results, the change of zeta potential value from 31.3 ± 0.4 mV to -15.03 ± 0.38 indicates successful conjugation of Angiopep-2 to the Ti@FeAu Nanoparticles.

Table 1. Surface potential values before and after Ti@FeAu Nanoparticles modification.

Formulation	**Zeta potential(mV)**
Ti@FeAu Nanoparticles	-31.3±0.4
Ti@FeAu-Ang Nanoparticles	-15.03±0.38

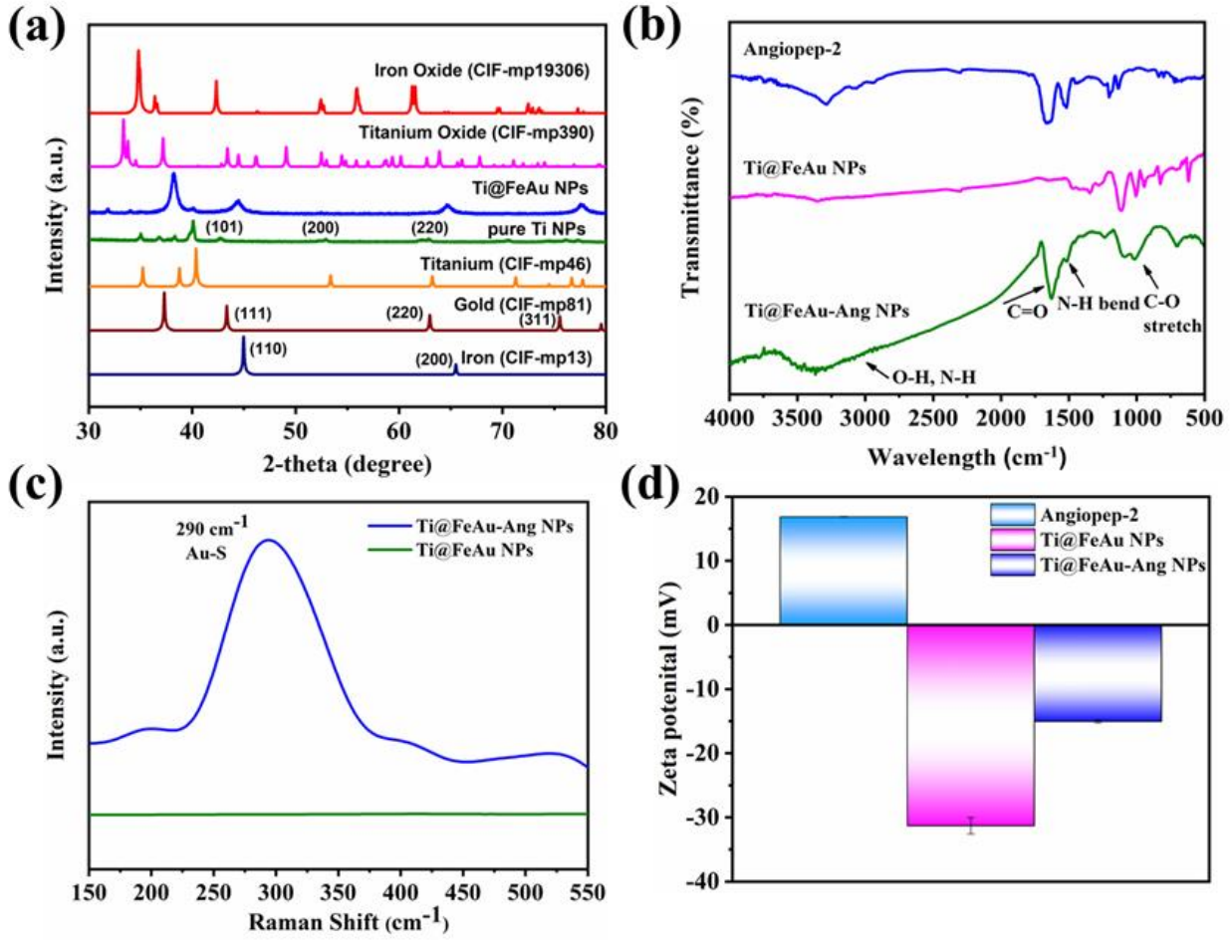

Figure 2. Characterization of Ti@FeAu core-shell Nanoparticles and Ti@FeAu-Ang Nanoparticles. (a) XRD analysis of Ti@FeAu Nanoparticles, (b) FTIR spectrum of Angiopep-2, Ti@FeAu Nanoparticles, and Ti@FeAu-Ang Nanoparticles, (c) Raman spectra before and after modification of the Ti@FeAu Nanoparticles with Angiopep-2, (d) Zetasizer graphs illustrating the zeta potential of Angiopep-2, Ti@FeAu Nanoparticles, and Ti@FeAu-Ang Nanoparticles.

3.2. Analysis of magnetic properties of Ti@FeAu and Ti@FeAu-Ang Nanoparticles

The magnetic properties of nanoparticles were studied using SQUID. The maximum temperature of the system was 300K as highlighted in ZFC/FC curve and is the blocking temperature (TB). The magnetization direction of nanoparticles is not constant when the

temperature of the system is lower than the TB, therefore, the magnetization decreases with temperature. Ferromagnetic materials lose spontaneous magnetic moment and change from an ordered to a disordered paramagnetic phase (Figure 3a). The hysteresis curved passed through origin and coercive force or residual magnetization was not observed which indicates that superparamagnetism was observed both in the presence as well as absence of Angiopep-2 conjugation. The saturation magnetization of Ti@FeAu and Ti@FeAu-Ang nanoparticles was 4.07 and 2.18 emu/g, respectively. Collectively, these results indicate that the conjugation of Angiopep-2 to nanoparticles had little effect on the magnetic properties of Ti@FeAu nanoparticles (Figure 3b).

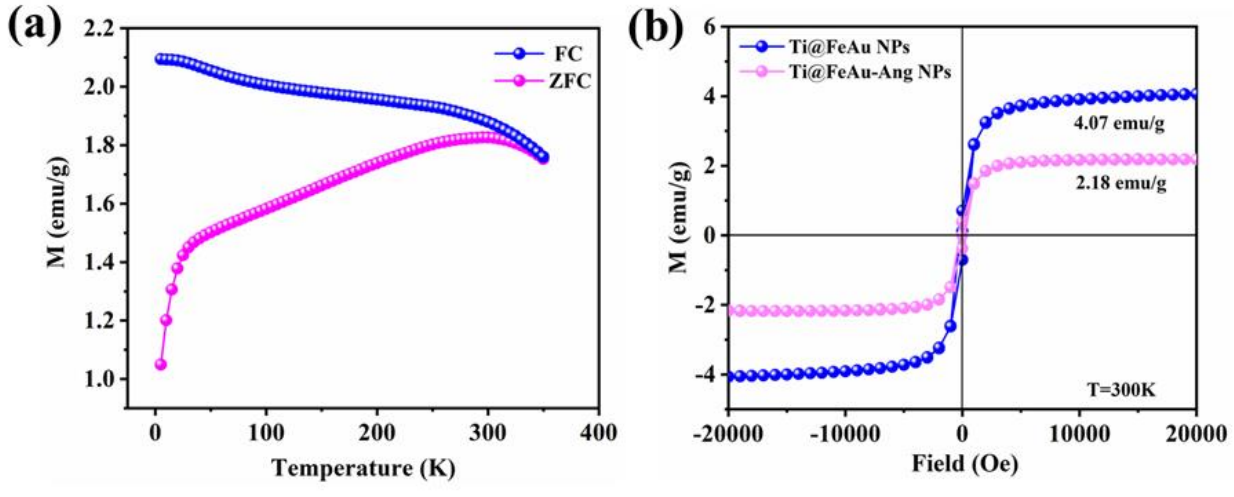

Figure 3. SQUID analysis of Ti@FeAu Nanoparticles. (a) ZFC/FC curves of Ti@FeAu Nanoparticles, (b) Hysteresis curves (M-H curves) of Ti@FeAu Nanoparticles and Ti@FeAu-Ang Nanoparticles.

3.3. Hyperthermia generation during magnetic field stimulation

Ti@FeAu Nanoparticles were diluted at different concentrations and exposed to AMF. The results highlighted that the amount of heat released was proportional to the concentration of the Nanoparticles used. The temperature was maintained at 36.2 °C at 2.5 mg mL^{-1} concentration of

Ti@FeAu Nanoparticles, highlighting the small concentration of the Nanoparticles that may be employed for targeting cancer cells (Figure 4). Further, the temperature of the solution increased to 38.2 °C at 10 mg mL^{-1} Nanoparticles concentration, highlighting the ability of Ti@FeAu Nanoparticles to generate magnetic field-induced hyperthermia towards cancer theranostics.

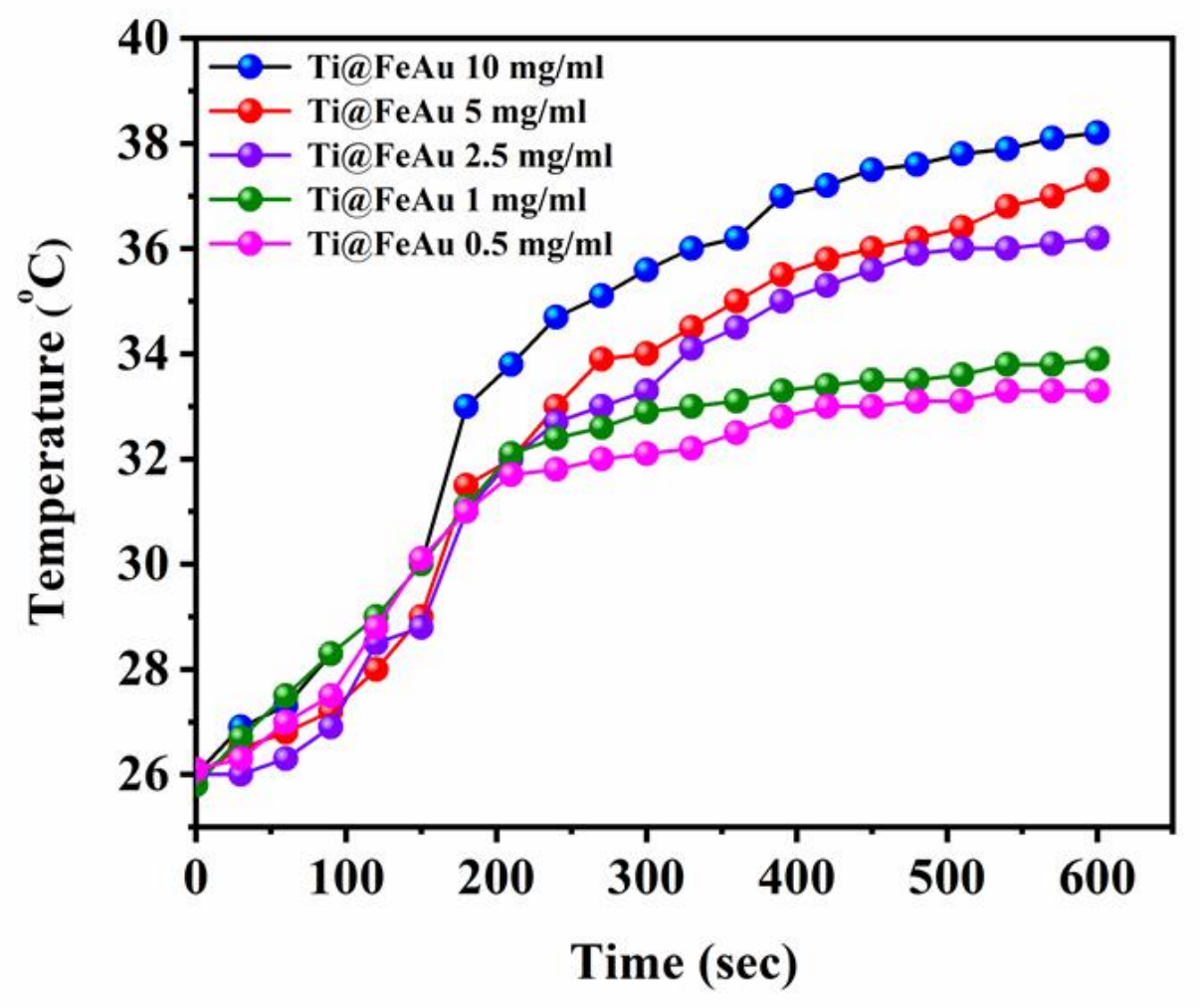

Figure 4. Temperature elevation of Ti@FeAu Nanoparticles at different concentrations of Ti@FeAu Nanoparticles over 10 minutes.

3.4. Ti@FeAu-Ang Nanoparticles as a contrast agent

Magnetic resonance spectroscopy was used to confirm the application of Ti@FeAu or Ti@FeAu-Ang Nanoparticles as a negative contrast agent. The image contrast varied as a function

of nanoparticle concentration. For both Ti@FeAu and Ti@FeAu-Ang experimental groups, Nanoparticles displayed a higher signal intensity at 0.03125 mg mL^{-1}, and lower signal intensity at 0.5 mg mL^{-1}, demonstrating the suitability of peptide-conjugated nanoparticles can change the image contrast in a dose-dependent manner (Figure 5a). Moreover, conjugation of Angiopep-2 did not hinder the ability of Ti@FeAu Nanoparticles to act as a contrast agent. The inverse relationship was obtained between the concentration of Ti@FeAu or Ti@FeAu-Ang Nanoparticles and MRI signal intensities. From the concentration-dependent plots, the transverse relaxation rate (r_2) of Ti@FeAu and Ti@FeAu-Ang Nanoparticles were 10.815 and 12.357 mg^{-1} s^{-1}, respectively (Figure 5b). These results suggest that Ti@FeAu-Ang Nanoparticles can be used as contrast agents in medical resonance imaging.

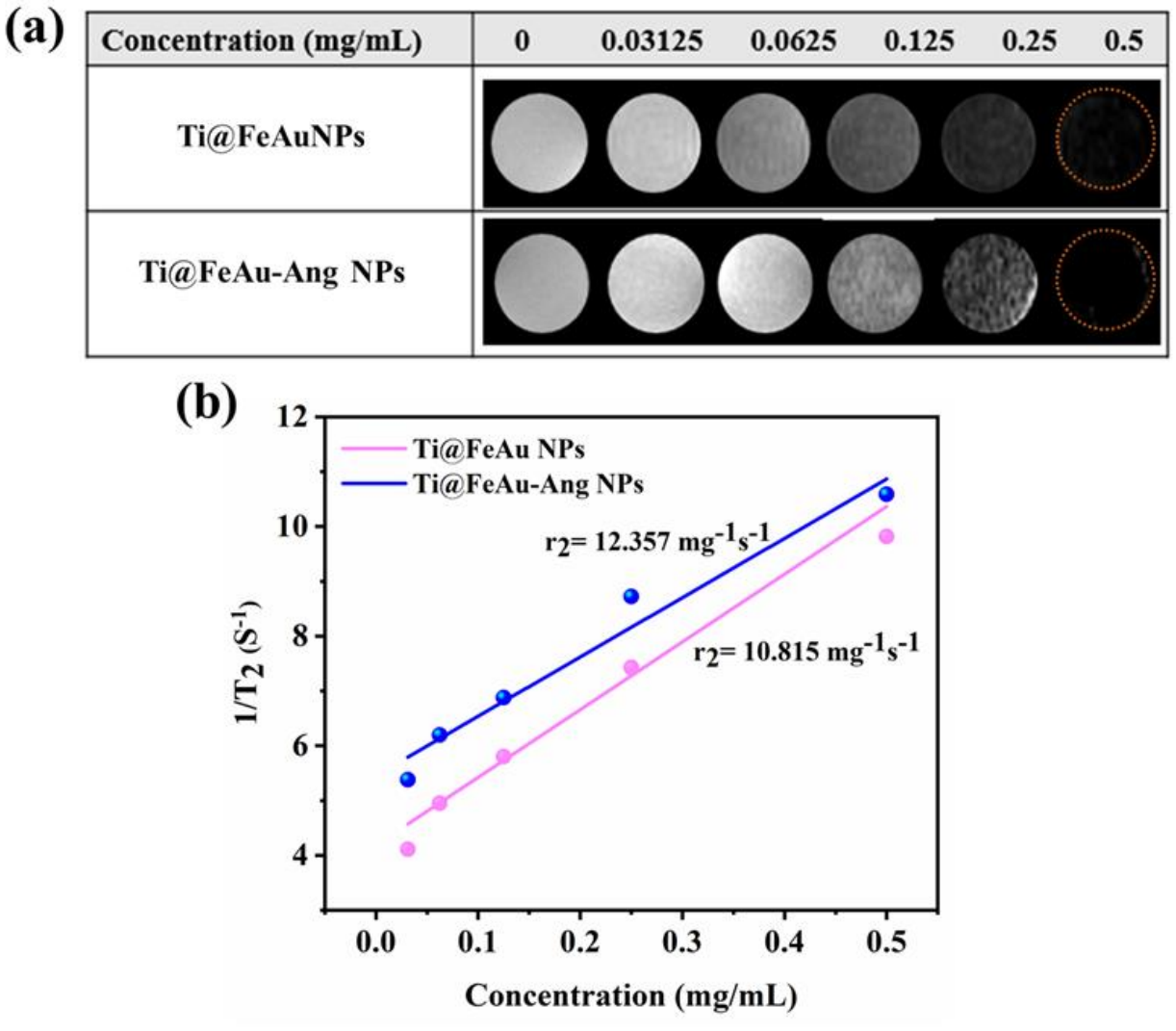

Figure 5. MRI images of Ti@FeAu Nanoparticles and Ti@FeAu-Ang Nanoparticles. (a) To investigate modulation of image contrast, various concentrations of Ti@FeAu and Ti@FeAu-Ang Nanoparticles in agarose were used. (b) A graph illustrating the direct relationship between Ti@FeAu Nanoparticles concentration and transverse relaxation time for Ti@FeAu and Ang-Ti@FeAu, respectively.

3.5. *In-vitro* cytotoxicity

MTT assay was performed to evaluate the *in-vitro* cytotoxicity of nanoparticles. L929 fibroblasts exhibited a small difference in cell viability towards Ti@FeAu Nanoparticles and Ti@FeAu-Ang at 1 mg mL^{-1} concentration (Figure 6a). Moreover, no significant difference in the

viability of L929 between experimental groups containing Ti@FeAu Nanoparticles and Ti@FeAu-Ang Nanoparticles was observed, which reveals that angiopep-2 conjugation does not affect the biocompatibility of Ti@FeAu Nanoparticles. Targeting brain tumor using Ti@FeAu-Ang Nanoparticles is the key objective of this study, therefore the cell viability was evaluated by incubating C6 glioma cells in the presence of Ti@FeAu and Ti@FeAu-Ang Nanoparticles. The cell viability results show that the concentration of Ti@FeAu/Ti@FeAu-Ang Nanoparticles is inversely proportional to the cell viability (Figure 6b). Moreover, at 250 µg mL^{-1} concentration, the viability decreased to 69 and 62 % for Ti@FeAu Nanoparticles and Ti@FeAu-Ang Nanoparticles, respectively. Besides, a lower concentration of Ti@FeAu-Ang Nanoparticles can be expected to display low side-effects towards healthy stroma surrounding brain tumors. Interestingly, at an identical concentration of 1mg mL^{-1}, Ti@FeAu-Ang Nanoparticles cytotoxicity towards L929 and C6 glioma cells was found to be 48% and 70%, which may be attributed to higher uptake by C6 glioma cells owing to Angiopep-2 conjugation of the nanoparticles. This result demonstrates that Ti@FeAu-Ang Nanoparticles have a targeted cytotoxicity effect on glioma cells.

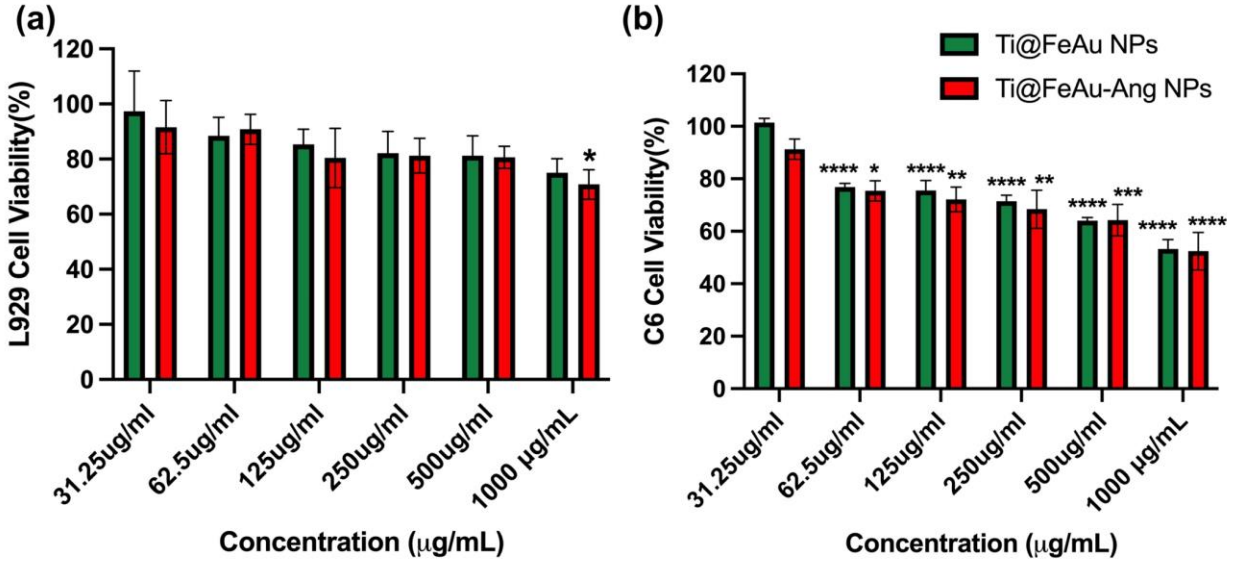

Figure 6. Cytotoxicity of Ti@FeAu Nanoparticles and Ti@FeAu-Ang Nanoparticles by MTT

assay. (a) L929 and (b) rat glioma cells (C6). Statistical analysis was performed using one-way ANOVA on Graphpad Prism 9.

3.6. Evaluation of nanoparticles ingestion

We anticipated that the conjugation of Angiopep-2 to Ti@FeAu Nanoparticles would result in enhanced cellular uptake of Ti@FeAu-Ang Nanoparticles, resulting in higher cell death. Therefore, time-based optical imaging was performed to prove the visualization of Ti@FeAu Nanoparticles and Ti@FeAu-Ang Nanoparticles endocytosis. The optical imaging results showed that the cellular uptake of Ti@FeAu-Ang Nanoparticles by C6 cells was higher than Ti@FeAu Nanoparticles (Figure 7a). In addition to verify these findings, C6 cells and L929 fibroblasts cells were incubated with Ti@FeAu Nanoparticles and Ti@FeAu-Ang Nanoparticles, and the elemental composition was evaluated using ICP-MS (Figure 7b).

These above results revealed that cellular uptake of Nanoparticles was nearly 1.2-fold higher for the experimental group comprising of Ti@FeAu-Ang Nanoparticles than Ti@FeAu Nanoparticles. Moreover, the C6 cells displayed higher nanoparticle uptake as compared to L929 cells. We hypothesize that this enhanced uptake by glioma cells may be due to the presence of LRP-1 on C6 cells. However, further experiments will be needed to verify this.

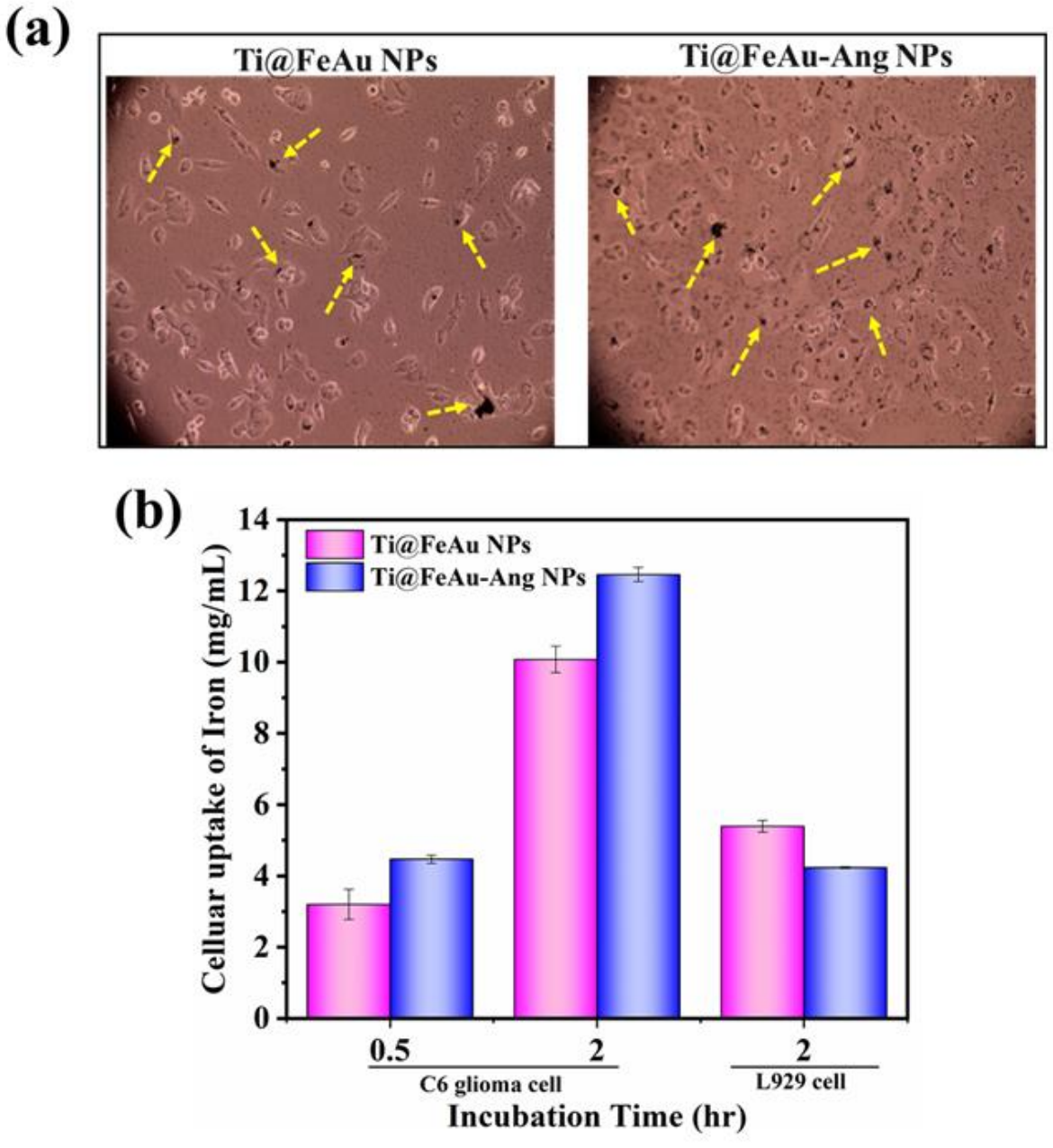

Figure 7. Cellular uptake of C6 cells incubated with different Nanoparticles (a) Optical microscopy analysis and (b) ICP-MS analysis. The arrows in Fig. 7a indicate localization of Ti@FeAu or Ti@FeAu-Ang nanoparticles.

3.7. Hyperthermia treatment of Ti@FeAu and Ti@FeAu-Ang Nanoparticles on C6 glioma cells

To analyse the effect of Ti@FeAu Nanoparticles-produced hyperthermia on glioma cell death, cells were incubated with Ti@FeAu Nanoparticles and Ti@FeAu-Ang Nanoparticles, and

both experimental groups were stimulated using AMF (Figure 8). Time-based magnetic stimulation was carried out to determine the optimum time for magnetic field exposure to induce cancerous cell death. These findings showed that the percentage of cell survival decreased when the period of magnetic field exposure increases in Ti@FeAu Nanoparticles and Ti@FeAu-Ang Nanoparticles-treated experimental groups. The higher accumulation of Ti@FeAu-Ang Nanoparticles in cells can be expected to contribute to enhanced hyperthermia effect, resulting in higher cancer cell death. After 15 minutes of magnetic stimulation, cell viability decreased to 21.2 % and 11.4 % in experimental groups containing Ti@FeAu Nanoparticles and Ti@FeAu-Ang Nanoparticles, respectively. The result confirmed that large numbers of cells were necrotized due to the accumulation of Nanoparticles inside the cancer cells during hyperthermia treatment.

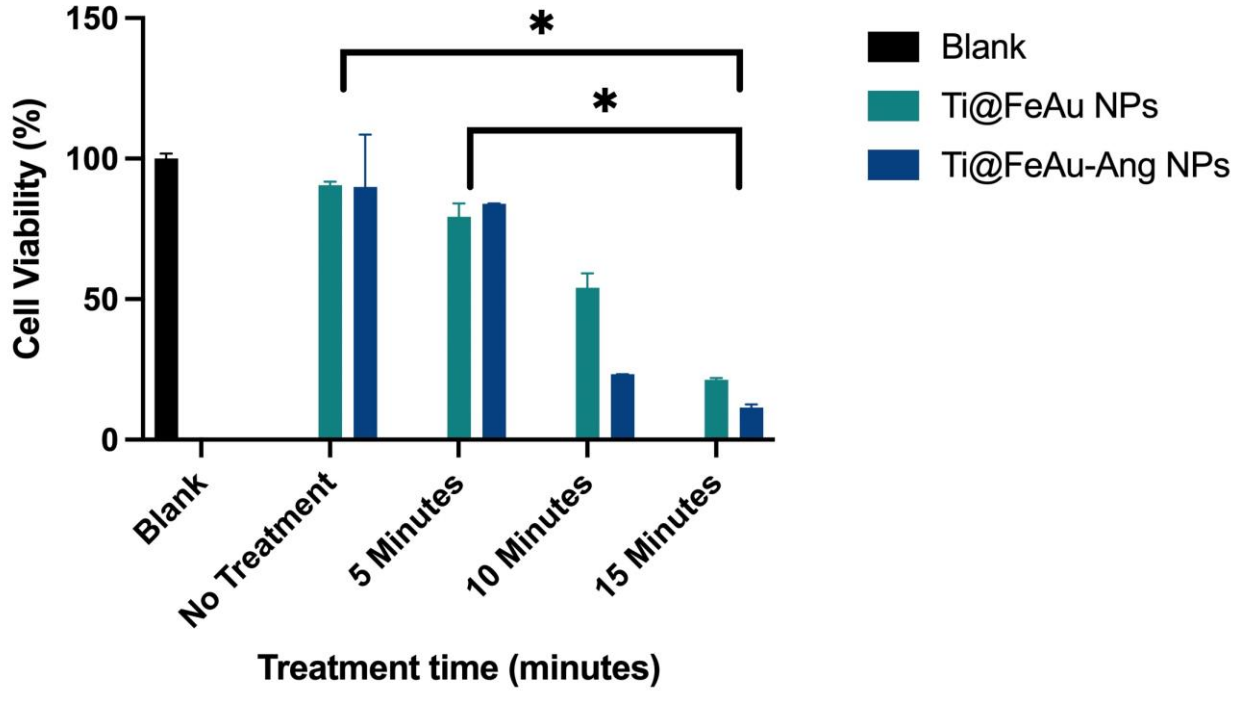

Figure 8. *In vitro* analysis of the effect of AMF-induced hyperthermia on C6 glioma cell viability.Statistical difference between experimental groups was performed using one-wa ANOVA test on graphpad prism 9.

3.8. Application of Ti@FeAu-Ang Nanoparticles as a tumor contrast agent in a rat model

Our previous experimental results showed that Ti@FeAu Nanoparticles and Ti@FeAu-Ang Nanoparticles could be used as a contrast agent by modulation of T_2 relaxation time, and Ti@FeAu Nanoparticles/Ti@FeAu-Ang Nanoparticles shows specific ingestion by C6 cells. To study the image contrast efficiency of Ti@FeAu-Ang Nanoparticles in brain tumor, 200 µL (5 mg mL^{-1}) of the Ti@FeAu-Ang Nanoparticles were injected intravenously into the rat and then subjected to 7T MRI after 2 hours of post-injection. As shown in (Figure 9), the tumor site became dark and distinct after i.v injection of Ti@FeAu-Ang Nanoparticles. However, poor contrast was observed in pre-injected groups accompanied with poor tumor visualization. These results revealed that Ti@FeAu Nanoparticles can be employed as MRI contrast agents to facilitate tumor identification owing to Angiopep-2 conjugation by glioma cells.

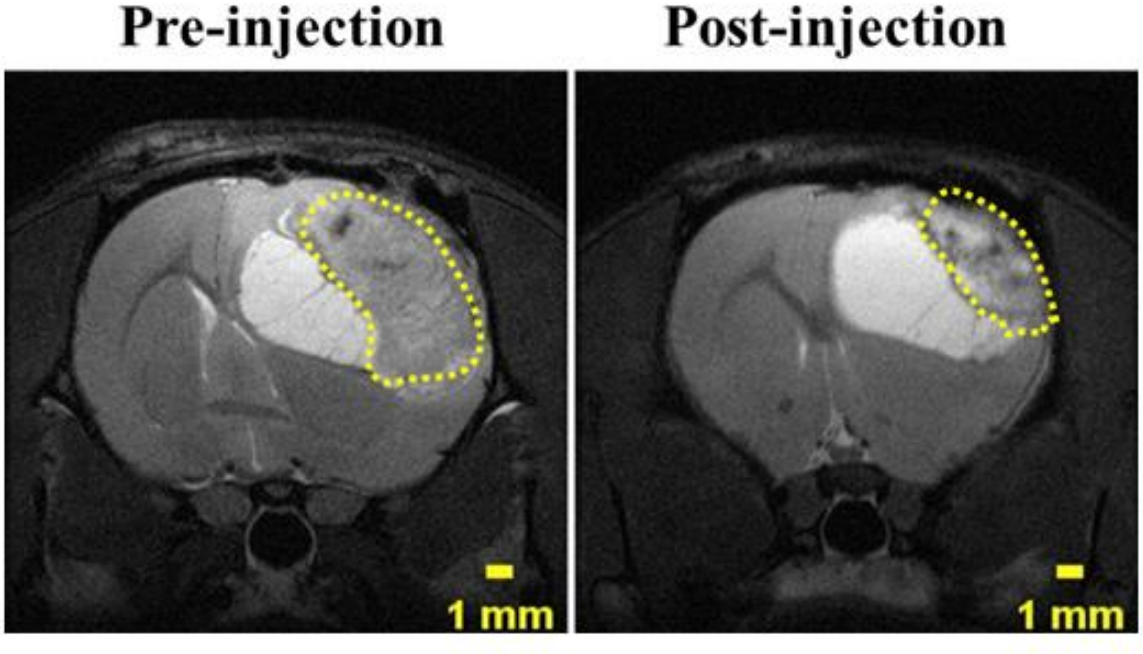

Figure 9. *In-vivo* MRI imaging of tumor before and 2 hours after injection of Ti@FeAu-Ang Nanoparticles

3.9. *In-vivo* therapeutic efficacy of Ti@FeAu-Ang core-shell Nanoparticles

The potential of magnetic nanoparticles to produce hyperthermia and elevated ingestion of peptide-conjugated magnetic core-shell Nanoparticles by C6 cells motivated us to study the anti-cancer effect of Ti@FeAu-Ang Nanoparticles *in-vivo*. As shown in (Figure 10a), the control group displayed an enormous increase in tumor growth with average volume of 475 mm^3. The experimental groups containing FeAu Nanoparticles were subjected to AMF inhibited tumor growth with an average volume of 190 mm^3. These findings were consistent with our previous study where tumor volume decreases because of hyperthermia facilitated cell death triggered by FeAu magnetic nanoparticles[35]. Compared to FeAu Nanoparticles +AMF, an experimental group containing Ti@FeAu Nanoparticles +AMF also exhibited tumor shrinkage to 143 mm^3. The experimental groups containing Ti@FeAu-Ang Nanoparticles +AMF showed a 10-fold (average tumor volume of 40 mm^3) decrement in tumor volume compared to the control group.

Immunohistochemical staining examination was performed for glioma tissues from the above-mentioned experimental groups (Figure 10b). H&E staining was used to identify the morphology of cells and tissues which helps to detect necrosis or microvascular proliferation of cells. These results showed that active cell proliferation was observed in control groups, whereas experimental groups containing Ti@FeAu-Ang Nanoparticles + AMF displayed higher tumor cell necrosis as compared to Ti@FeAu Nanoparticles + AMF. The observed results can be explained due to the higher cellular intake by tumor cells, which resulted in higher necrosis. Major organs like heart, liver, spleen, kidney, and lung were analysed using H&E staining for safety evaluation of as-prepared nanoparticles to validate the toxicity to normal tissues *in-vivo* (Figure 10c). Compared to the control group, no significant organ damage and biological changes were observed for Ti@FeAu-Ang Nanoparticles-treated groups. Consequently, Ti@FeAu-Ang Nanoparticles + AMF displayed no significant side effects on the treated rats.

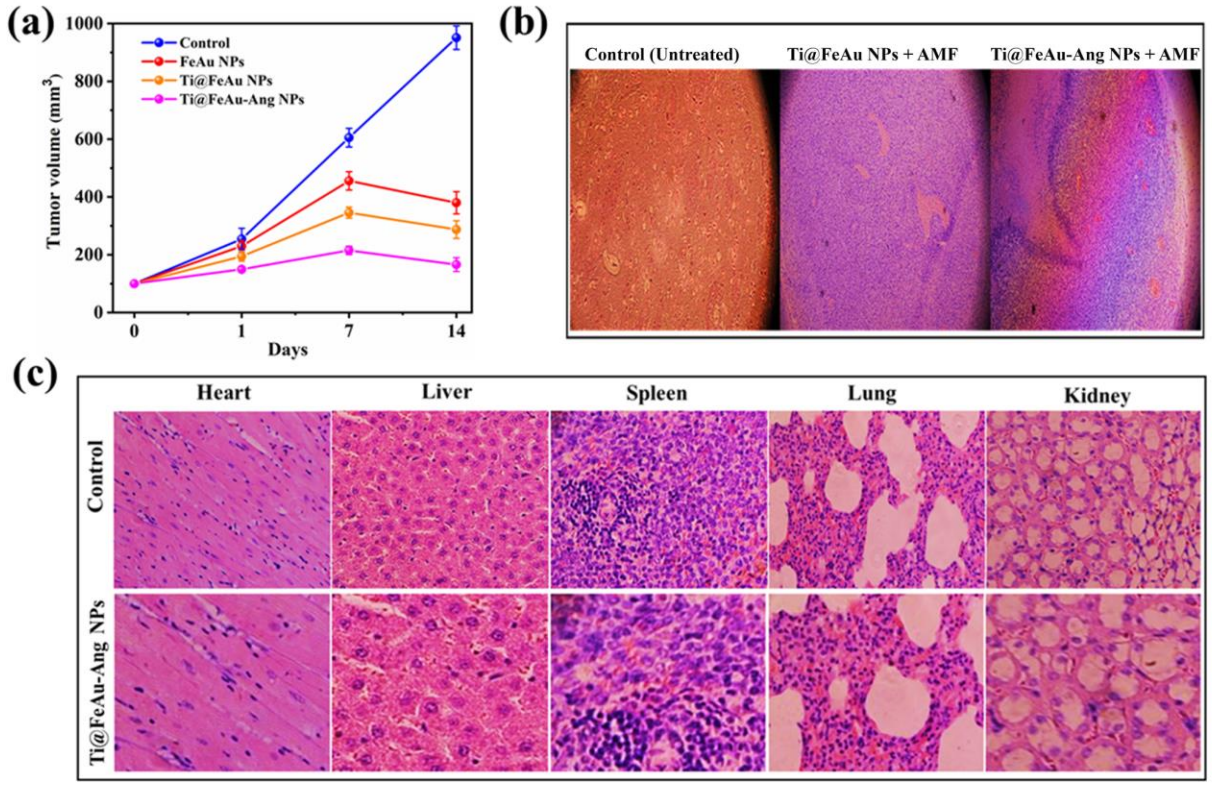

Figure 10. *In-vivo* therapeutic analysis. **(a)** The tumor volume measurement after AMF stimulation of control and experimental groups over 14 days, (b) immunohistochemical analysis (H&E staining) of glioma tissues from rat brain for observing the morphological changes between control and experimental groups, (c) optical micrograph of H&E-stained sections vital organs including heart, liver, spleen, kidney, and lungs from the control and Ti@FeAu-Ang Nanoparticles +AMF groups to assess anatomical safety. Statistical analysis of the data was performed using Kruskal-Wallis test.

4. Conclusions

This study reports the fabrication and application of Ti@FeAu-Ang Nanoparticles as a theranostic platform for imaging and hyperthermia-assisted cancer therapy simultaneously. Upon exposure to AMF, Ti@FeAu-Ang Nanoparticles exhibited superparamagnetic behaviour and

generated hyperthermia in a concentration-dependent manner. Targeted delivery of Ti@FeAu-Ang Nanoparticles was observed which resulted in higher C6 glioma cell death. Ti@FeAu-Ang Nanoparticles also exhibited enhanced MRI imaging contrast when used at 5 mg mL^{-1}, highlighting the suitability of this platform for medical imaging. Besides, our results show that the Ti@FeAu-Ang Nanoparticles triggered more than 90 % glioma cell death after 15 minutes of AMF stimulation. The selective cellular uptake of Angiopep-2-decorated Ti@FeAu Nanoparticles by glioma cells makes this a promising platform for *in-vivo* tumor therapy. *In-vivo* results confirmed that intravenous injection of Ti@FeAu Nanoparticles on rats effectively inhibited tumor growth with AMF stimulation without damaging vital organs. Therefore, the CPP-conjugated core-shell Nanoparticles can serve as a platform for simultaneous nanotheranostics and advanced imaging.

Declaration

The authors declare that they have no conflicting financial interests.

Acknowledgment

The authors are grateful for the financial support provided by the Ministry of Science and Technology of Taiwan (MOST 107-2221-E-027-014; MOST 108-2628-E-027-003-MY3); part of the Development and Reform Commission of Jilin Province (2017C059-5), and the Science and Technology Department of Jilin Province (20200401091GX). Graphical abstract was prepared using Biorender.com. Technical assistance from the Precision Analysis and Material Research Center of National Taipei University of Technology (Taipei Tech) is appreciated.

References

1. F. Lu, Z. Pang, J. Zhao, K. Jin, H. Li, Q. Pang, L. Zhang and Z. Pang, *Int J Nanomedicine*, 2017, **12**, 2117-2127.
2. S. Shirvalilou, S. Khoei, S. Khoee, N. J. Raoufi, M. R. Karimi and A. Shakeri-Zadeh, *Chem Biol Interact*, 2018, **295**, 97-108.
3. H. Gao, J. Qian, S. Cao, Z. Yang, Z. Pang, S. Pan, L. Fan, Z. Xi, X. Jiang and Q. Zhang, *Biomaterials*, 2012, **33**, 5115-5123.
4. S. Huang, J. Li, L. Han, S. Liu, H. Ma, R. Huang and C. Jiang, *Biomaterials*, 2011, **32**, 6832-6838.
5. T. Lin, P. Zhao, Y. Jiang, Y. Tang, H. Jin, Z. Pan, H. He, V. C. Yang and Y. Huang, *ACS Nano*, 2016, **10**, 9999-10012.
6. J. Ahlawat, G. Guillama Barroso, S. Masoudi Asil, M. Alvarado, I. Armendariz, J. Bernal, X. Carabaza, S. Chavez, P. Cruz, V. Escalante, S. Estorga, D. Fernandez, C. Lozano, M. Marrufo, N. Ahmad, S. Negrete, K. Olvera, X. Parada, B. Portillo, A. Ramirez, R. Ramos, V. Rodriguez, P. Rojas, J. Romero, D. Suarez, G. Urueta, S. Viel and M. Narayan, *ACS Omega*, 2020, **5**, 12583-12595.
7. T. D. Brown, N. Habibi, D. Wu, J. Lahann and S. Mitragotri, *ACS Biomater Sci Eng*, 2020, **6**, 4916-4928.
8. H. Gao, C. Chu, Y. Cheng, Y. Zhang, X. Pang, D. Li, X. Wang, E. Ren, F. Xie, Y. Bai, L. Chen, G. Liu and M. Wang, *ACS Appl Mater Interfaces*, 2020, **12**, 26880-26892.
9. Y. Cui, Q. Xu, P. K. Chow, D. Wang and C. H. Wang, *Biomaterials*, 2013, **34**, 8511-8520.
10. J. Ren, S. Shen, D. Wang, Z. Xi, L. Guo, Z. Pang, Y. Qian, X. Sun and X. Jiang, *Biomaterials*, 2012, **33**, 3324-3333.
11. E. Eriste, K. Kurrikoff, J. Suhorutsenko, N. Oskolkov, D. M. Copolovici, S. Jones, P. Laakkonen, J. Howl and U. Langel, *Bioconjug Chem*, 2013, **24**, 305-313.
12. H. Gao, S. Zhang, S. Cao, Z. Yang, Z. Pang and X. Jiang, *Mol Pharm*, 2014, **11**, 2755-2763.
13. M. M. Khan, N. Filipczak and V. P. Torchilin, *J Control Release*, 2021, **330**, 1220-1228.
14. X. Wang, Z. Xiong, Z. Liu, X. Huang and X. Jiang, *Sci Rep*, 2018, **8**, 12827.
15. X. Ji, H. Wang, Y. Chen, J. Zhou and Y. Liu, *AMB Express*, 2019, **9**, 165.
16. X. Wang, G. Liu, N. Chen, J. Wu, J. Zhang, Y. Qian, L. Zhang, D. Zhou and Y. Yu, *ACS Appl Mater Interfaces*, 2020, **12**, 12143-12154.
17. A. Hanini, L. Lartigue, J. Gavard, K. Kacem, C. Wilhelm, F. Gazeau, F. Chau and S. Ammar, *Journal of Magnetism and Magnetic Materials*, 2016, **416**, 315-320.
18. Z. Nemati, J. Alonso, L. M. Martinez, H. Khurshid, E. Garaio, J. A. Garcia, M. H. Phan and H. Srikanth, *The Journal of Physical Chemistry C*, 2016, **120**, 8370-8379.
19. S. Zhao, X. Yu, Y. Qian, W. Chen and J. Shen, *Theranostics*, 2020, **10**, 6278-6309.
20. L. Beola, L. Asin, C. Roma-Rodrigues, Y. Fernandez-Afonso, R. M. Fratila, D. Serantes, S. Ruta, R. W. Chantrell, A. R. Fernandes, P. V. Baptista, J. M. de la Fuente, V. Grazu and L. Gutierrez, *ACS Appl Mater Interfaces*, 2020, **12**, 43474-43487.
21. J. Pan, P. Hu, Y. Guo, J. Hao, D. Ni, Y. Xu, Q. Bao, H. Yao, C. Wei, Q. Wu and J. Shi, *ACS Nano*, 2020, **14**, 1033-1044.
22. E. Alphandery, A. Idbaih, C. Adam, J. Y. Delattre, C. Schmitt, F. Guyot and I. Chebbi, *J Control Release*, 2017, **262**, 259-272.
23. R. Das, N. Rinaldi-Montes, J. Alonso, Z. Amghouz, E. Garaio, J. A. Garcia, P. Gorria, J. A. Blanco, M. H. Phan and H. Srikanth, *ACS Appl Mater Interfaces*, 2016, **8**, 25162-25169.
24. C. S. Schneider, G. F. Woodworth, Z. Vujaskovic and M. V. Mishra, *Radiother Oncol*, 2020, **142**, 43-51.
25. R. Gupta and D. Sharma, *ACS Chem Neurosci*, 2019, **10**, 1157-1172.

26. S. Kaushik, J. Thomas, V. Panwar, H. Ali, V. Chopra, A. Sharma, R. Tomar and D. Ghosh, *ACS Applied Bio Materials*, 2020, **3**, 779-788.
27. S. D. Anderson, V. V. Gwenin and C. D. Gwenin, *Nanoscale Res Lett*, 2019, **14**, 188.
28. Y. Du, X. Liu, Q. Liang, X. J. Liang and J. Tian, *Nano Lett*, 2019, **19**, 3618-3626.
29. P. Yadav, C. Zhang, A. K. Whittaker, K. Kailasam and A. Shanavas, *ACS Biomater Sci Eng*, 2019, **5**, 6590-6601.
30. Y. Q. Li, M. Xu, U. Dhawan, W. C. Liu, K. T. Wu, X. R. Liu, C. Lin, G. Zhao, Y. C. Wu and R. J. Chung, *Int J Nanomedicine*, 2018, **13**, 5499-5509.
31. C. N. Elias, J. H. C. Lima, R. Valiev and M. A. Meyers, *JOM*, 2008, **60**, 46-49.
32. E. D. de Avila, B. P. Lima, T. Sekiya, Y. Torii, T. Ogawa, W. Shi and R. Lux, *Biomaterials*, 2015, **67**, 84-92.
33. W. F. Oliveira, I. R. S. Arruda, G. M. M. Silva, G. Machado, L. Coelho and M. T. S. Correia, *Mater Sci Eng C Mater Biol Appl*, 2017, **81**, 597-606.
34. Z. Xie, S. Chen, Y. Duo, Y. Zhu, T. Fan, Q. Zou, M. Qu, Z. Lin, J. Zhao, Y. Li, L. Liu, S. Bao, H. Chen, D. Fan and H. Zhang, *ACS Appl Mater Interfaces*, 2019, **11**, 22129-22140.
35. M. A. Behnam, F. Emami, Z. Sobhani and A. R. Dehghanian, *Iran J Basic Med Sci*, 2018, **21**, 1133-1139.